Contribution of the different aerosols species to the aerosol mass load and optical depth present over the northeastern tropical Atlantic

I. Chiapello, Gilles Bergametti, Bernadette Chatenet, François Dulac, Isabelle Jankowiak, Catherine Liousse, Emmanuel Santos Soares

JOURNAL OF GEOPHYSICAL RESEARCH, VOL. 104, NO. D4, PAGES 4025–4035, FEBRUARY 27, 1999

Contribution of the different aerosol species to the aerosol mass load and optical depth over the northeastern tropical Atlantic

Isabelle Chiapello,[1,2] Gilles Bergametti,[1] Bernadette Chatenet,[1] Francois Dulac,[3] Isabelle Jankowiak,[4] Catherine Liousse,[3] and Emmanuel Santos Soares[5]

Abstract. Simultaneous ground-based measurements of chemical composition, size distribution, and column optical thickness at 670 nm of atmospheric aerosols have been performed at Sal Island (Cape Verde) during the winter season when African dust is transported in the lower troposphere. Mineral dust and, occasionally, sea salt dominate the aerosol mass load, whereas the excess sulfates plus the carbonaceous aerosol (particulate organic matter and black carbon) contributions to the mass load remain lower than 5% on average. We compute the total aerosol optical depth (AOD) by combining optical properties derived from measured size distributions and vertical concentration profile of each aerosol type estimated from surface elemental concentrations and meteorological observations. Results are very consistent with direct Sun photometer measurements. This allows us to derive the chemical apportionment of AOD in this region: mineral dust from Africa controls the total AOD and generally dominates AOD even in the absence of dust outbreak; on average, sea salt, excess sulfate, and carbonaceous aerosols all together only contribute to an averaged background AOD of 0.04 at 670 nm.

1. Introduction

The radiative effect of the tropospheric aerosol represents one of the major uncertainties in modeling the radiative forcing of climatic changes [*Intergovernmental Panel on Climate Change*, 1994; *Penner et al.*, 1994; *Schwartz and Andreae*, 1996]. This effect depends both on the concentrations and on the optical properties of aerosols, the latter being linked to the aerosol chemical composition and size distribution. In fact, the estimation of the contribution of the global aerosol system to the radiative forcing is highly uncertain, mainly because the various aerosol species exhibit both strong spatial and temporal variabilities of their concentrations and physicochemical properties. It is necessary to provide atmospheric and radiative models with appropriate data in order to test, refine, and validate calculations of aerosol optical effects [*Penner et al.*, 1994; *Quinn et al.*, 1995]. In this context, experimental studies performed over selected regions and focused on simultaneous measurements of concentrations, physicochemical and optical properties for each aerosol type present are highly valuable [*Liousse et al.*, 1997; *Hegg et al.*, 1997].

[1]Laboratoire Interuniversitaire des Systèmes Atmosphériques, Universités Paris 7-Paris 12, Créteil, France.
[2]Now at Laboratoire d'Optique Atmosphérique, Université des Sciences et Technologies de Lille, Villeneuve d'Ascq, France.
[3]Laboratoire des Sciences du Climat et de l'Environnement, UMR CEA-CNRS, Gif sur Yvette, France.
[4]Laboratoire d'Optique Atmosphérique, Université des Sciences et Technologies de Lille, Villeneuve d'Ascq, France.
[5]Servico Nacional de Meteorologia i Geofisica, Sal, Cape Verde.

Paper number 1998JD200044.
0148-0227/99/1998JD200044$09.00

The aerosol optical depth (AOD) constitutes one of the pertinent indicators of the direct radiative effect produced by the aerosol particles [*Penner et al.*, 1994; *Sokolik and Toon*, 1996]. It can be measured directly from groundlevel stations using Sun photometers [*Prospero et al.*, 1979; *Tanré et al.*, 1988; *Nakajima et al.*, 1996; *Holben et al.*, 1998]. It can also be retrieved, with a spatial and temporal coverage suitable for global scale analysis, from satellite data over oceanic regions [*Dulac et al.*, 1992; *Jankowiak and Tanré*, 1992; *Husar et al.*, 1997; *Moulin et al.*, 1997a]. Nevertheless, AOD measurements reflect the integrated optical effect of the various aerosol species present in the atmospheric column over a given location. Thus it is of the highest interest to obtain simultaneously data sets of concentrations and properties of the different aerosol types in order to evaluate their relative contribution to the measured AOD. With such a data set, *Hegg et al.* [1997] show that the carbonaceous aerosols rather than sulfates dominate the AOD off the mid-Atlantic coast of the United States.

The purpose of this study is to evaluate how the major aerosol species over the northeastern tropical Atlantic contribute to the aerosol optical depth. Over this region, satellites record the highest AOD of the world ocean [*Husar et al.*, 1997], suggesting that the aerosol particles could lead to an important regional radiative forcing. Especially, the role of the North African mineral dust known to be present in large quantities in this area [e.g., *Prospero and Carlson*, 1972; *Jaenicke and Schütz*, 1978; *Jankowiak and Tanré*, 1992; *Moulin et al.*, 1997b] has to be specified. Indeed, it is now recognized that the impact of the desert dust cannot be ignored in the evaluation of the anthropogenic climate forcing [*Andreae*, 1996] because, among other reasons, a significant fraction of their emissions could be derived from human land degradation, especially in the Sahelian region [*Tegen and Fung*, 1995; *Tegen et al.*, 1996; *Sokolik and Toon*, 1996].

Our approach consists in retrieving the AOD from measurements of concentrations and size distributions, calculation of optical properties, and estimations of the vertical profiles from radiosounding for each major aerosol type (desert dust, excess sulfates, seasalt, and carbonaceous particles) observed in the tropical Atlantic off Senegal. The results of AOD calculations are constrained by matching them with simultaneous Sun photometer measurements. The agreement observed between computed and measured AOD will allow us to discuss the contribution of each aerosol type to the AOD.

2. Method

For a given aerosol type, the AOD (τ) is the vertical integral of the aerosol extinction coefficient (K_e) on the whole atmospheric column:

$$\tau = \int_0^\infty Ke(z)dz \quad (1)$$

K_e accounts for both scattering and absorption of solar light by the aerosol particles present in the atmosphere. It has dimension of the inverse of a length and varies as a function of the altitude z with particle concentration in the air column. If C is the aerosol mass concentration in g m^{-3}, then

$$Ke(z) = \sigma e(z) x C(z) \quad (2)$$

with σ_e specific extinction cross section in m^2 g^{-1} if K_e is in m^{-1}.

Assuming that the aerosol is mainly externally mixed (i.e., the different particle species reside mainly in different particle populations), the measured AOD can be considered to be the sum of the AOD due to each different aerosol specie i:

$$\tau = \sum_i \tau_i \quad (3)$$

If we assume that the optical properties of each aerosol specie are preserved over the vertical column, then

$$\tau = \sum_i (\sigma i \int_0^\infty Ci(z)dz) \quad (4)$$

To calculate the AOD, it is thus necessary to determine for each aerosol type (1) its vertical profile of mass concentration and (2) its specific extinction cross section, which depends on its chemical nature and size distribution.

2.1. Ground-Based Mass Measurements

Since December 1991, a continuous aerosol monitoring station has been operating on Sal Island (16°45'N, 22°57'W; altitude, 62 m), the most northeastern island of the Cape Verde archipelago. This archipelago is located in the northeastern tropical Atlantic, 500 km west off the African coast. Recent studies dealing with the seasonality of the African dust transport [*Chiapello et al.,* 1995], and with the sources of desert aerosols [*Chiapello et al.,* 1997a; *Caquineau,* 1997], have provided precise information, allowing to define the experimental strategy to use for this study. Especially, the seasonal variability and transport process of the North African dust have been investigated from the long-term daily records [*Chiapello et al.,* 1995]. It has been shown that the highest mineral dust concentrations at Sal occur in winter due to a low-layer transport process in the trade winds (from the sea-surface up to 1.5-3 km). On the contrary, in summer, dust is mainly transported above the trade wind layer in the so-called Saharan Air Layer (located between 1.5-3 km and 5-7 km height) [*Prospero and Carlson,* 1972; *Carlson and Prospero,* 1972]. This high-altitude transport does not significantly affect the concentrations measured during summer at ground level at Sal [*Chiapello et al.,* 1995]. These results indicate that a pertinent comparison between the vertically integrated AOD measurements and the aerosol concentrations measured at ground level can only be performed during the winter period at Sal. In complement to aerosol concentration monitoring [*Chiapello et al.,* 1997a], we performed three winter field experiments in December 1991, January 1994, and from December 1994 to February 1995 in order to realize particle size distribution and optical measurements.

2.1.1. Aerosol concentrations. During these experiments, aerosol samples were collected by bulk filtration on 0.4 μm pore-size Nuclepore filters with a nominal flow rate of about 1 m^3 h^{-1}. The period for aerosol collection generally corresponded to that during which the AOD measurements were performed (between 2 and 9 hours during the daytime). To quantify the elemental mass concentrations of the different aerosol species, the samples were analyzed by X ray fluorescence spectrometry (SIEMENS SRS 303), following the method previously described by *Losno et al.* [1987] and modified by *Chiapello et al.* [1997b]. The chemical analysis focused on the elements that can be considered as tracers of the three major aerosol species in this region: Al and Si (which are good indicators of the mineral dust of African origin), Na (tracer of sea salt concentrations) and S (to characterize excess sulfate aerosols, i.e., non-sea salt sulfates produced by gas-particle conversion). The precision of the measurements, depending mainly on the concentration level, ranges between 3 and 10%.

From December 1991 to March 1992, bulk filtration was also performed on quartz fiber filters for subsequent carbonaceous aerosol analyses, with a sample time step ranging between 2 and 5 days. Particulate carbon concentrations in the aerosol were determined by thermal analysis [*Cachier et al.,* 1989] of quartz filters. The filters were subjected to HCl vapors for 24 hours to remove carbonates. The carbon remaining on the filters after this treatment is referred to as total atmospheric particulate carbon (TC). Both total and black carbon measurements were performed on filter aliquots by coulometric titration with a Ströhlein Coulomat®702C with an uncertainty of the order of 5%. The black carbon (BC) fraction is analyzed after the thermal removal of the organic compounds at 340°C during the 120 min under pure oxygen. Organic carbon (OC) is assumed to be the difference between TC and BC. It must be recalled, however, that the BC and OC separation is method dependent [*Reid et al.,* 1998]. Intercomparisons between different methods showed a 10-35% range of difference.

2.1.2. Aerosol size distributions. The mass-size distribution of the noncarbonaceous aerosol species was retrieved by using cascade impactor sampling. We used an EGAI 80 low-volume cascade impactor [*Bergametti et al.,* 1982] operating at a nominal flow rate of 1 m^3 h^{-1}. The EGAI 80 impactor is a single-jet circular cascade impactor with five stages and a final backup filter. 0.4 μm pore-size Nuclepore filters were used as impaction surfaces for both the final backup filter and the five impactor stages for which 50% aerodynamic equivalent cutoff diameters are 8.75, 3.90, 1.95, 1.25, and 0.65 μm at nominal flow rate. The sampling duration varied from few hours (in dusty conditions) to

24 hours (in clear conditions). The parameters of the mass-size distribution were retrieved by using lognormal assumptions and a fitting procedure accounting both for the usual errors (i.e., bounce-off and fluctuations of flow rate) and for the respective collection efficiencies of the different cascade impactor stages [*Gomes et al.*, 1990].

2.2. Optical Ground-Based Measurements

Since October 1994, Sal Island has been one of the permanent sites of the ground-based aerosol monitoring network described by *Holben et al.* [1998]. An automatic Sun-tracking spectral radiometer, model 318A from CIMEL Electronique, Paris, has been settled there. The Sun photometer has a 1.2° full angle field of view and measures the direct sunlight as well as the sky radiance. Between the two spectral bands most suitable for aerosol studies (i.e., 440 and 670 nm), we choose to use the 670 nm band, since it is most reliable in terms of calibration and least contaminated by Rayleigh contribution. To discriminate small clouds from an important dust plume, a Sun measurement is based on three spectral observations (triplets) taken 30 s apart. Clouds are supposed to be more inhomogeneous than dust and involve an observable variation in the raw digital data. The routine Sun measurement protocol is based on triplet observations with at most 15 min intervals in between. This instrument is first intercalibrated with a reference Sun photometer. Then the calibration is checked with the Langley data collection made by the radiometer each morning and afternoon between an optical air mass of 2 and 7. The AOD is estimated with an accuracy of ± 0.02.

2.3. Meteorological Data

Analysis of the meteorological rawindsonde soundings (i.e., vertical profiles of temperature and relative humidity) was used to characterize the structure of the atmosphere. At Sal Island, the rawindsonde soundings (from surface pressure to 300 hPa) are performed daily (around 1000 LT, local time) by the Cape Verdean Meteorological Service. Moreover, basic meteorological parameters were recorded at ground level with 1-hour time intervals.

3. Determination of Parameters Controlling Aerosol Optical Depth

3.1. Vertically Integrated Mass Concentrations

3.1.1. Mass concentrations at ground level. The mineral dust concentrations were deduced from silicon concentrations, considering that Si represents one third of the total mineral aerosol concentration in agreement with both soil models of *Bowen* [1966] and *Vinogradov* [1959]. Generation of aerosols by wind erosion generally yields compositional fractionation of parent soils with likely impoverishment in Si [e.g., *Rahn*, 1976], but data on Si concentrations in Saharan aerosols are missing to constrain this ratio. Including analytical errors on Si concentration measurement, one can assume a relative uncertainty of ± 20% on the total dust content.

Sodium concentrations were used to approach the sea salt mass concentrations. However, when dust transport occurs, this element also presents a significant crustal component, which needs to be subtracted. By looking at the very intense dust events [*Chiapello*, 1996], it has been shown that the crustal sodium (Na_c) concentration can be estimated by the relation

$$Na_c = 0.10 \times Al \quad (5)$$

where 0.10 is the Na/Al concentration ratio in desert dust. This value is very close to that recommended by the *Bowen* [1966] soil model (Na/Al = 0.09).

Thus we can estimate the marine sodium concentration Na_m from the measured sodium by subtracting its soil-derived component:

$$Na_m = Na - Na_c \quad (6)$$

The sea salt concentration is then computed by using the relative mass abundance of Na (0.33) in sea water (sw) [*Brewer*, 1975]:

$$(\text{sea salt}) = 3 \times (Na_m) \quad (7)$$

The third main aerosol specie whose concentration needs to be quantified is excess sulfate aerosols. The excess sulfates are defined as the sulfates produced by gas-particle conversion. In this region the excess sulfates could have two main origins: anthropogenic (from SO_2 oxidation) and/or biogenic (from the oxidation of the dimethylsulfide (DMS) emitted at the sea surface). Besides these excess sulfates, sulfates can also exhibit significant contributions due to mineral dust and sea salt, both containing sulfur. Since our measurements provide only elemental sulfur concentrations, these contributions from sea salt and soil-derived particles must be subtracted to retrieve excess sulfates. The following procedure is used: using a sea water model, the sea salt component of sulfur S_{SS} can be easily determined by the classical relation

$$S_{ss} = (S/Na)_{sw} \times (Na_m) \quad (8)$$

with $(S/Na)_{sw} = 0.082$ in mass [from *Brewer*, 1975]. The non-sea salt sulfur concentration S_{nss} is then

$$S_{nss} = S - S_{ss} \quad (9)$$

To determine the crustal component of the sulfur (S_c), an approach based on the size distribution of the non sea salt sulfur was used. Two distinct modes are found (not shown), one with a mass-median diameter of about 0.2 μm and the other with a mass-median diameter greater than 1 μm equal to that of Al [*Chiapello*, 1996]. It is likely that the submicronic mode contains excess sulfur and that the second is of crustal origin. The S/Al mass concentration ratio in mineral dust was calculated from the S_{nss}/Al mass ratio in the dust particle mode, leading, for dusty conditions (Al> 30 μg m^{-3}), to a value of 0.01, which is very close to that recommended by the *Bowen* [1966] soil model (S/Al=0.0099). Thus the excess sulfur concentration S_{xs} was calculated from

$$S_{xs} = S_{nss} - S_c \quad (10)$$

with $S_c = 0.01 \times Al$, the crustal sulfur mass concentration.

By assuming that in the troposphere the excess sulfates are mainly neutralized by ammonium to form various forms of ammonium sulfates [*Clarke et al.*, 1987; *Koutrakis and Kelly*, 1993] the excess sulfate concentration is estimated, according to the $(NH_4)_2SO_4$ stoechiometry, to be 4.19 times that of excess sulfur. Accounting for the various hypotheses involved in the computation and for the analytical uncertainties, it may be

considered that the excess sulfate concentration is retrieved within 30%.

The fourth main aerosol specie, which may contribute to the aerosol optical depth in Sal Island, is the carbonaceous aerosol. The main source for these particles would be the African biomass burning sources at the beginning of the dry season (November to January). A minor impact could be due to fossil fuel sources originating from southern Europe and/or northwestern Africa such as for sulfate particles. Carbonaceous aerosol is usually separated in two fractions, the black carbon (BC), and the organic carbon (OC) particles. The organic carbon fraction is always predominant in the carbon mixture [*Cachier*, 1998]. Let us note that in the following calculation, instead of (OC), we will consider the particulate organic matter (POM) which includes in addition to carbon, hydrogen atoms, oxygen atoms, and minor amounts of other species [*Liousse et al.*, 1996] with POM/OC=1.3.

Figure 1 presents the temporal variations of the concentrations of these aerosol species during the 1994-1995 winter experiment at Sal. Since no carbonaceous aerosol measurement was available during this experiment, we reported the average concentration from measurements over the period December 1991 to March 1992. One can observe several intense African dust events, with concentrations of mineral dust higher than 200 μg m^{-3}. Sea salt, excess sulfates, and carbonaceous aerosol concentrations were strongly lower during the whole period. The sea salt concentrations roughly ranged between 10 and 30 μg m^{-3}, most of the excess sulfate concentrations values were lower than 5 μg m^{-3}, and the average carbonaceous aerosol concentration was 1.5 μg m^{-3} (i.e., average concentrations of 0.53 (±0.37) μg m^{-3} for BC and 0.98 (±0.86) μg m^{-3} for POM).

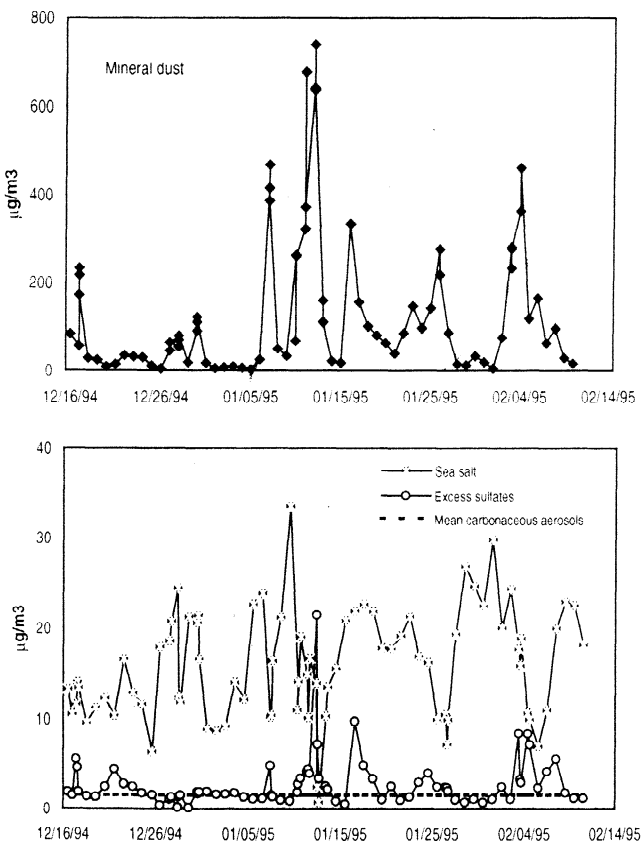

Figure 1. Daily variations of the mineral dust, sea salt, and excess sulfates concentrations recorded at ground level at Sal Island from mid-December 1994 to mid-February 1995. Carbonaceous aerosol (sum of black carbon and particulate organic matter) average concentration from measurements at Sal Island from December 1991 to March 1992 is reported.

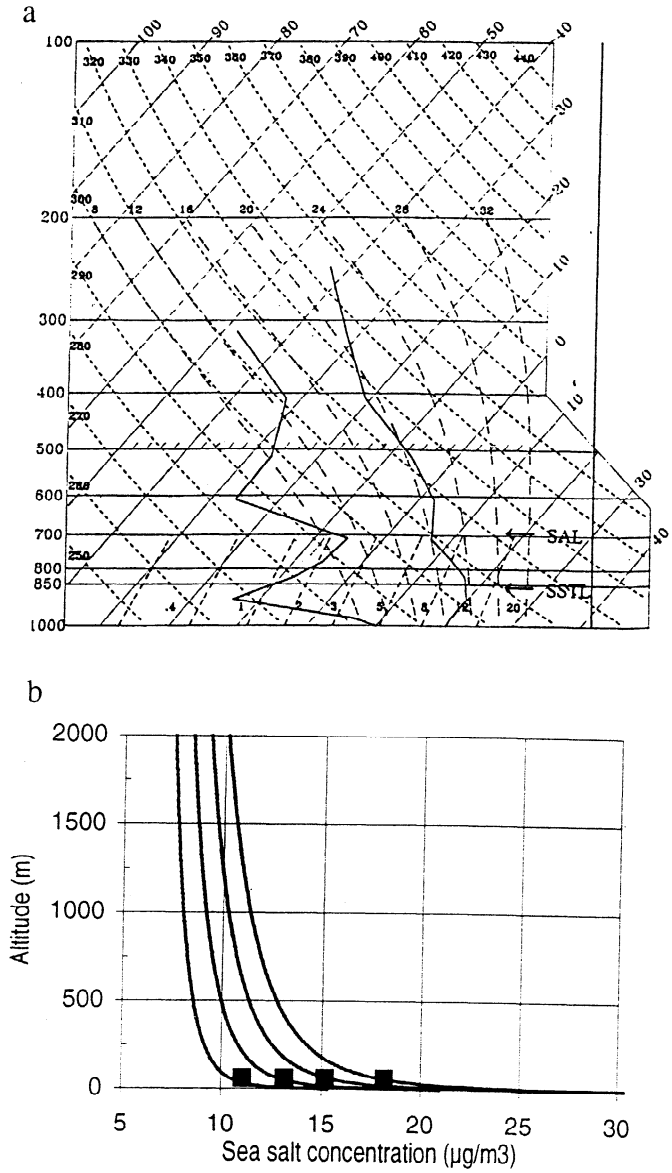

Figure 2. (a) Example of a typical emagram obtained at Sal Island during an African dust event in winter. The vertical profiles of water-mixing ratios and potential temperatures are indicated, as well as the Saharan Air Layer and sub-saharan transition layer limits. These data are derived from the soundings performed by the Servico Nacional de Meteorologia i Geofisica at Sal Island. (b) Vertical profiles of sea salt concentrations derived from the *Blanchard and Woodcock* [1980] relation for wind speed of 6, 7, 8, and 9 m/s, and mean values of sea salt concentrations measured for the corresponding wind speeds at Sal Island at 62 m altitude during the 1995 winter experiment.

3.1.2. Vertical repartitions. The thickness of the mineral dust layer was determined by using the vertical profiles of potential temperature and mixing ratio of the water vapor deduced from the daily meteorological radiosoundings performed at Sal. *Carlson and Prospero* [1972] have shown that in summer

the Saharan Air Layer could be identified from discontinuities of these two parameters. Indeed, this layer is characterized as an isentropic layer in which the potential temperature is nearly constant (40° to 45°C); the water vapor mixing ratio varies very little with altitude inside the layer with typical values of 2 to 4 g kg^{-1}. We applied this approach to determine, for each day of the campaign, the thickness of the various layers. Figure 2a presents a typical example of emagram obtained at Sal during an African dust event. In winter, as mentioned above, the intense dust events (i.e., Si concentrations higher than 30 $\mu g\ m^{-3}$) are due to a dust transport at lower altitude [*Chiapello et al.*, 1995], in a layer called sub-Saharan transition layer (see Figure 2a). Its upper limit corresponds to the base of the Saharan Air Layer and range from altitudes of 1.5 to 3 km. Thus we used the discontinuities in potential temperature and mixing ratio of the water vapor to identify the boundaries of the sub-Saharan transition layer, where we assumed most of the dust mass to be located. Because of the poor vertical resolution of the radiosoundings the uncertainty in the determination of the dust layer thickness by this method is in the range 10 to 20%. Considering that after at least 500 km of transport the dust should be well mixed in this layer, we have assumed that the concentration of dust measured at ground level reflected the average dust concentration of the sub-Saharan transition layer. This is the most realistic assumption in absence of direct measurements of vertical profiles of dust concentrations. However, further investigations are needed to precise the degree of mixing of dust in the sub-Saharan transition layer. For the dust free and moderate dust situations (i.e., Si concentrations lower than 30 $\mu g\ m^{-3}$), we observed that the mean altitude of the dust layer needed to fit AOD measurements corresponds to the top of the Saharan Air Layer (located between 3 and 5.5 km altitude). Therefore in these situations we adopted the top of the Saharan Air Layer as the upper limit of the supposed well-mixed mineral dust layer. Nevertheless, we do not have enough information at this point to be sure that this assumption is really representative of the actual dust repartition.

Investigating the variability of the concentrations of excess sulfates at Sal in relation to three-dimensional air mass trajectories, we have previously shown [*Chiapello,* 1996] that high excess sulfate concentrations were observed for air masses originating from southern Europe or the industrial coastal regions of northwestern Africa, suggesting mainly anthropogenic sources. Their emissions being located at ground level and the involved transport process similar to that of African dust in winter, we have considered, as previously made for mineral dust, that the excess sulfates were well mixed inside the sub-Saharan transition layer. This has also been assumed for the vertical repartitions of carbonaceous aerosols, their sources in this region being most probably located over the African continent as well.

The vertical profile of sea salt particles is more complex to evaluate. Their emission is directly dependent on the local wind speed. This local origin induces a strong vertical gradient of the concentrations. *Blanchard and Woodcock* [1980] established, from a large number of measurements, a relation allowing to retrieve the vertical sea salt concentration as a function of the wind speed at sea level:

$$s=5(6.3 \times 10^{-6} H)^{(0.21-0.39 \log v)} \quad (11)$$

where s is mean sea salt concentrations ($\mu g\ m^{-3}$), H is altitude in meters, and v is wind speed at sea level ($m\ s^{-1}$).

This relation generally applies from 1 to 300 m altitude. However, for this study, this relation has been integrated up to 2000 m, altitude from which the sea salt concentration becomes negligible [*Blanchard and Woodcock*, 1980]. Figure 2b reports the computed vertical profiles of sea salt for different wind speeds. To test the validity of this relation, the mean sea salt concentrations measured at Sal at 62 m altitude for the corresponding wind speed have also been reported. A good agreement is observed between the mean measured concentrations and those established from the *Blanchard and Woodcock* [1980] relation. This relation has been used to compute the vertically integrated concentrations of sea salt between 62 m (altitude of the AOD measurements) and 2000 m.

3.2. Specific Extinction Cross Sections

Our calculation of the specific extinction cross section of each aerosol component (with the exception of carbonaceous aerosols) is based on the Mie theory, which allows us to derive the main optical properties of aerosols (aerosol extinction coefficient, phase function, single-scattering albedo, asymmetry factor, etc.) from their size distributions and complex index of refraction. The complex index of refraction $m= m_{RE} - im_{IM}$ consists of a real part m_{RE}, which is the ratio of the speed of light in a vacuum to the speed of light in the material, and an imaginary part m_{IM}, which is an absorption parameter characterizing the material. The complex index of refraction depends on the chemical nature of the particle. Experimental determinations of this index for the main aerosol species are found in the literature.

The size distribution of the aerosol is a determinant parameter to evaluate its optical properties. For this study, it is necessary to determine as accurately as possible the size distribution of each aerosol type in order to compute its specific extinction cross section. The size distributions obtained by cascade impactor are elemental mass-size distributions but can easily be transformed into number-size distributions (necessary for the Mie model input) assuming spherical particles and a density of 2.5 g cm^{-3} for mineral dust, 2.2 g cm^{-3} for sea salt, and 1.8 g cm^{-3} for excess sulfates. From *Jaenicke* [1987], for lognormal distributions

$$RN= RM(\exp(3\ (\ln\sigma)^2)^{-1}) \quad (12)$$

where RN and RM are the mean radius of the number and mass-size distribution, respectively, and σ is the standard deviation of

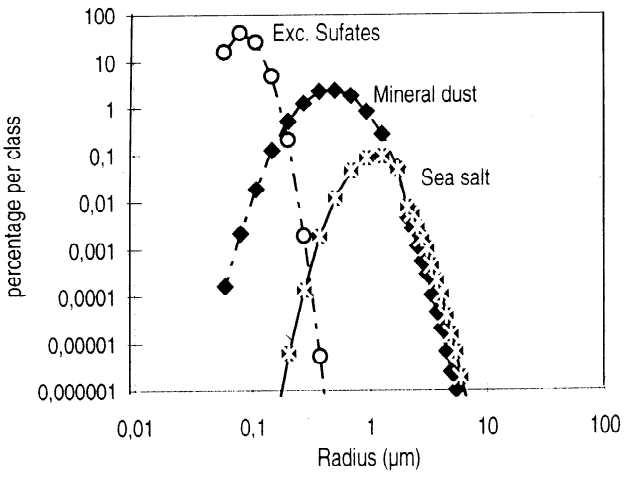

Figure 3. Typical number-size distributions of mineral dust, sea salt, and excess sulfates obtained at Sal Island from cascade impactor measurements.

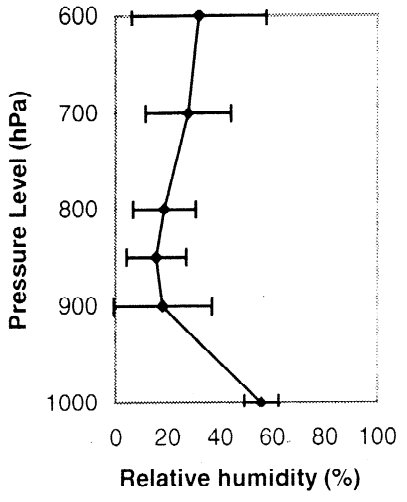

Figure 4. Vertical profile of the mean relative humidity (+/- sigma) obtained from the daily rawinsoundings performed at Sal Island between mid-December 1994 and mid-February 1995.

the size distribution. Figure 3 shows the typical size distributions obtained at Sal Island for major aerosol chemical components.

Figure 4 reports the vertical distribution of the mean relative humidity obtained from the daily rawinsoundings between mid-December 1994 and mid-February 1995. Because relative humidities greater than 60% were rarely observed (even at 1000 hPa, only 12% of the cases exhibit RH greater than 60% but lower than 75%), we will consider dry aerosol particles for the calculation of specific extinction cross sections.

3.2.1. Mineral dust. The real part of the refractive index generally used for the Saharan aerosol in the visible and close infrared is 1.55 [*Patterson et al.*, 1977; *Carlson and Benjamin*, 1980]. On the basis of the *Patterson et al.* [1977] study, we use as the imaginary part of the refractive index for Saharan dust, 4.10^{-3} at 670 nm.

Table 1a reports the median radius and standard deviation of the mass-size and number-size lognormal distributions for mineral dust (as traced by aluminum) and the specific extinction cross sections computed at 670 nm for each cascade impactor sample. The mean median radii are 0.89 μm and 0.44 μm for mass- and number-size distributions, respectively. The corresponding values of specific extinction cross sections range between 1.01 and 1.15 $m^2 g^{-1}$ at 670 nm. These values are comparable to the specific extinction cross sections determined for various desert aerosol models far from sources: such models reviewed by *Moulin et al.* [1997c] are in the range 0.58-0.82 $m^2 g^{-1}$, whereas the *Jankowiak and Tanré* [1992] model of dust over the Atlantic, derived from the *Shettle* [1984] model gives 1.03 $m^2 g^{-1}$ at 550 nm. These values are also consistent with the mass-scattering efficiencies of *Li et al.* [1996] obtained at Barbados during an experiment performed in April 1994, which range between 0.73 and 0.79 $m^2 g^{-1}$ at 530 nm.

3.2.2. Sea salt. The refractive index value of sea salt used in this study is that generally recommended, i.e., $1.38 - 4.26.10^{-9}i$ [Oceanic model, *World Climate Programme*, 1983; *d'Almeida et al.*, 1991].

As for mineral dust, the specific extinction cross sections of sea salt have been computed from the size distributions obtained from cascade impactor measurements. The results are reported in Table 1b: we observe monomodal size distributions centered at about 1.2 μm in radius. Other authors report sea salt distributions exhibiting also an accumulation mode around 0.1-0.2 μm representing about 10% of the total sea salt mass (e.g., *Quinn et al.*, 1996; *Howell and Huebert*, 1998).

The specific extinction cross sections, computed from our cascade impactor data, vary from 0.41 to 0.74 $m^2 g^{-1}$ (mean value of 0.52 $m^2 g^{-1}$). It must be noted that our values could be slightly underestimated due to the possible contribution of a submicron component of sea salt which has a larger specific extinction cross section. However, our values are in agreement with those of the oceanic aerosol model [*WCP*, 1983; *d'Almeida et al.*, 1991] computed at 550 nm (0.33 $m^2 g^{-1}$). This is also in agreement with the mass-scattering efficiencies computed at Barbados by *Li et al.* [1996] (0.3 to 0.5 $m^2 g^{-1}$ at 530 nm).

3.2.3. Excess sulfates. The refractive index value of sulfates used in this study is $1.53 - 6.10^{-3}i$, on the basis of the "water-soluble" (sulfate-like aerosol) aerosol model [*WCP*, 1983; *d'Almeida et al.*, 1991].

Even if in some situations excess sulfates present a bimodal mass-size distribution, due to a reaction of acidic sulfur species on sea salt (in clear conditions) or mineral dust (in dusty conditions) [*Chiapello*, 1996; *Dentener et al.*, 1996], we only considered the submicron mode for calculation of their specific extinction cross section. Indeed, because of the variability of the second mode, associated either with mineral dust or sea salt particles, it is difficult to take it into account from bulk samples, which do not provide information on size distributions. This approximation could result in some circumstances in a slight overestimate of the computed specific extinction cross section of excess sulfates. The median radius of the submicron mode, very stable, is 0.13 μm (for mass-size distribution), or 0.10 μm for number-size distribution (standard deviation of 1.25). The value of the corresponding specific extinction cross section is 1.01 $m^2 g^{-1}$. It must be noted that this specific extinction cross section has been obtained assuming a dry aerosol and considering only the excess sulfate ion. Taking into account the strong wavelength

Table 1a. Statistical Parameters of Mass and Number-Size Distributions of Mineral Dust (Derived From Cascade Impactors) Collected at Sal Island and Corresponding Specific Extinction Cross Sections (Computed From Mie Theory) at 670 nm

Sample Ref.	Al Conc. $\mu g/m^3$	Mass Median Radius, μm	Number Median Radius, μm	Geometric Standard Deviation	σ_e m^2/g 670 nm
IMP2 95	22	0.88	0.52	1.51	1.01
IMP6 95	25	0.86	0.37	1.69	1.15
IMP5 95	30	0.90	0.38	1.71	1.09
IMP3 95	51	0.88	0.46	1.59	1.06
IMP4 95	59	0.91	0.46	1.61	1.02
Mean	37	0.89	0.44	1.62	1.07

Aluminum concentration of each cascade impactor sample is indicated

Table 1b. Same as Table 1a for Sea Salt

Sample Ref.	Mass Median Radius, μm	Number Median Radius, μm	Geometric Standard Deviation	σ_e m^2/g 670 nm
IMP1 91	2.29	1.07	1.65	0.49
IMP1 95	1.96	1.68	1.25	0.41
IMP5 95	1.76	1.51	1.25	0.46
IMP2 95	1.69	1.45	1.25	0.48
IMP2 91	1.98	0.58	1.89	0.52
IMP6 95	1.48	1.27	1.25	0.56
IMP2 94	1.33	0.60	1.67	0.74
Mean	1.78	1.17	1.46	0.52

dependence of the sulfate specific extinction cross section, this value is comparable to that of the "water-soluble" model [*WCP*, 1983; *d'Almeida et al.*, 1991] (2.63 m^2 g^{-1} at 550 nm) and to those obtained in the Azores region by *Howell and Huebert* [1998] (0.6 to 2.6 m^2g^{-1} at 550 nm for dry aerosols).

3.2.4. Carbonaceous aerosols. For this study, no size distribution measurement was available for carbonaceous aerosols. Consequently, we computed their specific extinction cross sections from the values provided by *Liousse et al.* [1996] for black carbon and particulate organic matter at 300 and 550 nm (see Table 7 of this reference). This allows us to retrieve the Angström exponent of these two components (0.68 for black carbon and 0.92 for particulate organic matter), used to compute their specific extinction cross sections at 670 nm. The specific extinction cross sections obtained at 670 nm are 7.83 m^2 g^{-1} for black carbon and 3.34 m^2 g^{-1} for particulate organic matter. It can be noted that in the case of black carbon the computed specific extinction cross section accounts for both scattering and absorption, whereas the one computed for particulate organic matter only reflects the scattering, which can be considered as the dominant effect of this component [*Liousse et al.*, 1996].

3.2.5. Stratospheric aerosols. To account for the optical depth due to stratospheric aerosols, we used estimations based on ground-based lidar observations of the stratospheric aerosol layer by *Jäger et al.* [1995]. These authors reported for three different sites of the northern hemisphere stratospheric AOD around 0.01 at 532 nm for mid-1994 after decay of Mount Pinatubo aerosols. Taking into account the spectral variation of the stratospheric AOD (Angström coefficient of 1.52, computed from *Chazette et al.* [1995]), this value led to a contribution of stratospheric aerosol to the AOD of 0.007 at 670 nm.

4. Calculation of Total Aerosol Optical Depth

Taking into account the previous statements, we can compute the AOD from the vertically integrated mass concentrations and the mean values of the specific extinction cross sections of each aerosol specie. The total AOD is then inferred from the sum of the AOD computed for each aerosol specie.

4.1. Consistency With Measurements

Figure 5a compares the temporal variations of the computed AOD at 670 nm during the 1994-1995 winter experiment with the AOD measurements derived from the Sun photometer. To be consistent, the AOD measurements have been averaged for this comparison over the duration of the filtration samples (between 2 and 9 hours). Moreover, to avoid the influence of clouds, we selected the AOD measurements presenting good stability and a sufficient number of measures. Thus among the 57 days of the campaign (from December 16, 1994 to February 10, 1995), AOD measurements were not available for 6 days, and 14 days have been discarded, because of the poor confidence level of their AOD measurements. These days were characterized either by an insufficient number of measurements (less than 10) or by an important instability of the AOD (variations of a factor 2 to 10 over short periods of time, which are likely to be influenced by clouds). Measurements in the almucantar performed several times per day by the Sun photometer have been used as complements to

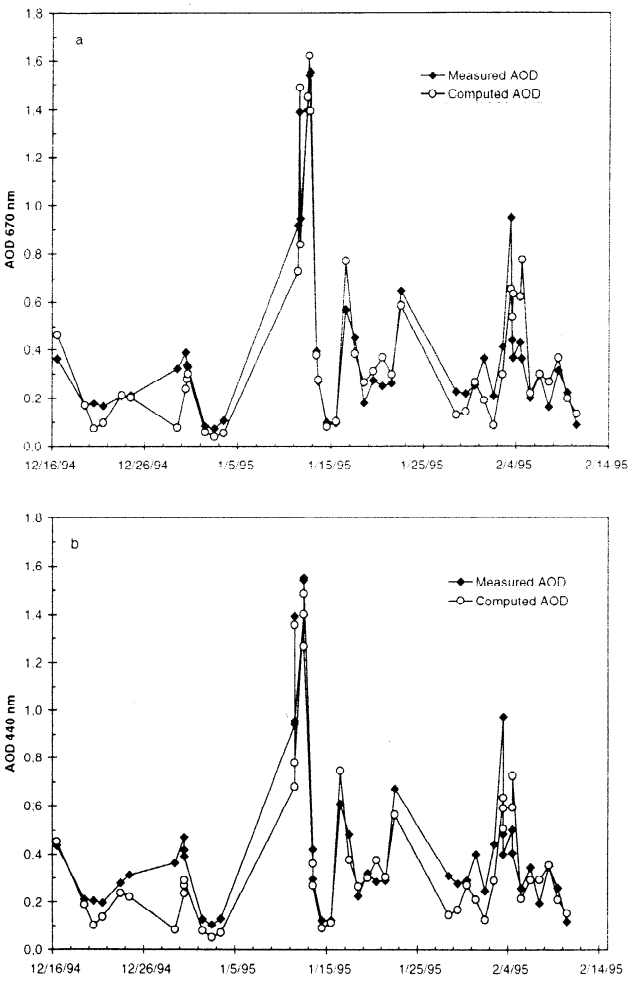

Figure 5. Temporal variations of the measured and computed aerosol optical depth at (a) 670 nm and (b) 440 nm from mid-December 1994 to mid-February 1995 at Sal Island.

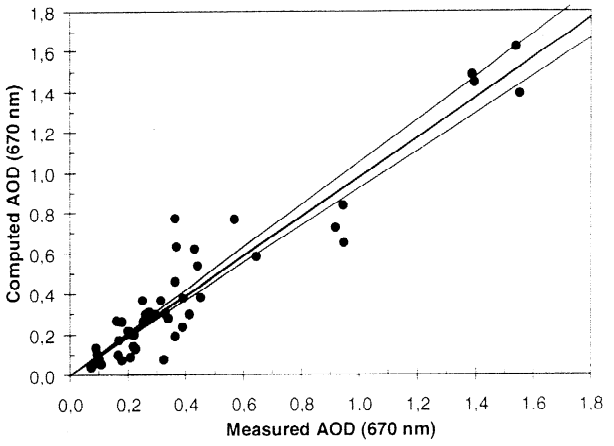

Figure 6. Relation between the computed aerosol optical depth and the measured aerosol optical depth at 670 nm. The thick line indicates the linear regression obtained from the 47 points. The slope is 0.98 ± 0.033 (r = 0.95), with a confidence index higher than 99%. The thin lines indicate the linear regressions obtained from the calculation of the aerosol optical depth with maximal and minimal values of the mineral dust and sea salt specific extinction cross sections (see Tables 1a and 1b).

confirm this classification. This approach allows us to reduce the influence of the uncertainties on AOD measurements in our calculation.

During these 2 months we encountered a large range of AOD values, including high AOD ranging between 0.4 and 1.6 and relatively low AOD values around 0.2. Figure 5a shows that the calculation allows us to reproduce satisfyingly the daily variations of the AOD at 670 nm, the computed AOD being in most cases in the same range as those directly measured. In order to check the consistency of our calculation, we also compare with measurements the AOD computed at 440 nm using the same procedure (Figure 5b).

For a more quantitative appreciation of the calculation, Figure 6 shows the computed AOD as a function of the AOD measurements. First, this comparison highlights good agreement between the computed and the measured values with a correlation coefficient greater than 0.9. The slight underestimate of the computed AOD (slope of 0.98) appears totally negligible, taking into account the uncertainties related to this comparison. Moreover, we have reported in these figures the linear regressions obtained by using the minimum and maximum values computed for mineral dust and sea salt specific extinction cross sections (see Table 1). It must be noted that these intervals include the linear regression with a slope of 1. As an explanation for the deviations of some computed AOD values along the linear regressions of Figure 6, it should be kept in mind that an important source of uncertainty for this calculation is related to the relatively crude estimation of the vertical profiles of each aerosol specie. Particularly, the hypothesis of a homogeneous mixed layer of mineral dust aerosols may introduce some deviations in our calculation, based only on the concentrations measured at ground level. Moreover, the 10 to 20% of error estimated for the aerosol layer thickness determinations (related to the vertical resolutions of the sounding) are probably responsible for some discrepancies as well. Besides this difficulty, the excellent agreement obtained for the computed AOD suggests that the main characteristics of the aerosol system are reasonably trapped by our measurements and assumptions.

4.2. Contribution of the Different Aerosol Species to Total Mass Load and Optical Depth

This approach allows an assessment of the contribution of the different aerosol species, i.e., mineral dust, sea salt, excess sulfates, and carbonaceous aerosols, to the total AOD. Figure 7 presents these relative contributions as a function of the measured AOD. First of all, this figure shows that for AOD higher than 0.4, the contribution of mineral dust to the total AOD is dominant and always greater than 80%. For lower AOD values, corresponding to clear or moderate dust situations, besides the contribution of the stratospheric aerosol, the effect of mineral dust remains in most cases larger than the one of other aerosol species. One can observe a limited number of cases for which carbonaceous aerosols and mineral dust contribute roughly identically to the global AOD. Tables 2a and 2b summarize the relative contributions of each aerosol specie, respectively, to the mass load and AOD. These results clearly show that mineral dust dominates both the aerosol mass load (average contribution of 71%) and the AOD (average contribution of 75%) in this region. Although sea salt particles contribute significantly to the aerosol mass load (24%), because of their small specific extinction cross sections their effect on the AOD remains limited (6% on average) and never exceeds 20%. Excess sulfates and carbonaceous aerosols, even if they account, on average, to only 5% of the total mass load represent, on average, 15% of the AOD. Despite limitations in our approach (not coincident carbonaceous concentration data and use of averaged aerosol optical properties) our results suggest that on average the relative contribution of carbonaceous aerosols to the AOD (12%) could be significantly larger than the relative contribution of excess sulfates (3%) in this region. Given the various sources of uncertainties, we estimate that the relative contribution of minor species to the total AOD is retrieved within a factor of 2, whereas the contribution of mineral dust is obtained with a relative uncertainty better than 30%.

To examine the absolute values of the AOD, Figure 8 shows the optical depth computed for each of the aerosol component as a function of the measured AOD. These results demonstrate that in this region the AOD is almost totally controlled by the variation of the mineral dust optical depth. Table 3 summarizes the averaged optical depth computed for each aerosol component. Besides mineral dust (and the contribution of stratospheric aerosols), our results show that carbonaceous aerosols, excess

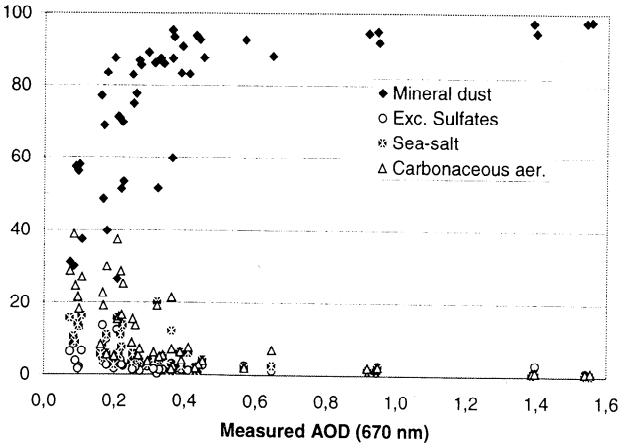

Figure 7. Relative contributions of the different aerosol components to the computed aerosol optical depth as a function of the measured aerosol optical depth at 670 nm.

Table 2a. Relative Contributions of Different Aerosol Species Measured at Ground Level at Sal Island to Total Mass Load

	Mineral Dust	Sea Salt	Excess Sulfates	Carbonaceous Aer.
Mean	71%	24%	2.9%	2.2%
Minimum	17%	0.11%	0.21%	0.20%
Maximum	99%	69%	14%	8.8%

Table 2b. Relative Contributions of Different Aerosol Species to Total Computed AOD at 670 nm at Sal Island

	Mineral Dust	Sea Salt	Excess Sulfates	Carbonaceous Aer.
Mean	75%	6.0%	3.0%	12%
Minimum	16%	0.04%	0.22%	0.9%
Maximum	98%	20%	14%	39%

Mean relative contribution of stratospheric aerosol (not reported in this table) is 4%.

sulfates, and sea salt only produce an average background AOD level of 0.04 at 670 nm. The carbonaceous aerosols (including black carbon and particulate organic matter) account on average to 50% of this background. The mean excess sulfates optical depth is 0.008 (maximum of 0.04), whereas the average optical depth of sea salt is 0.012 and never exceeds 0.02. So these results can be summarized in order of descending average contributions to the AOD as follows: mineral dust dominates, then carbonaceous aerosols, sea salt particles, and excess sulfates.

In the first approximation, i.e., neglecting aerosol absorption, AOD varies with the wavelength (λ) in the visible range following a power law

$$AOD(\lambda_1) / AOD(\lambda_2) = (\lambda_1 / \lambda_2)^{-\alpha} \quad (13)$$

where the Angström wavelength exponent α is related to the aerosol size distribution [*Junge*, 1963)]. It ranges from about zero (no spectral dependence of AOD) for large particles such as sea salt [*WCP*, 1983] and dust [*Moulin et al.*, 1997c] to 0.7-1.5 for carbonaceous aerosols [*Liousse et al.*, 1995, 1996] and between 1 and 2 for sulfates [*IPCC*, 1994]. This means that the relative contribution to total AOD from sulfates, and in a lesser extent the one from carbonaceous aerosols, increases when the wavelength decreases. Nevertheless, the mineral dust optical depth remains quite dominant over the whole visible spectrum.

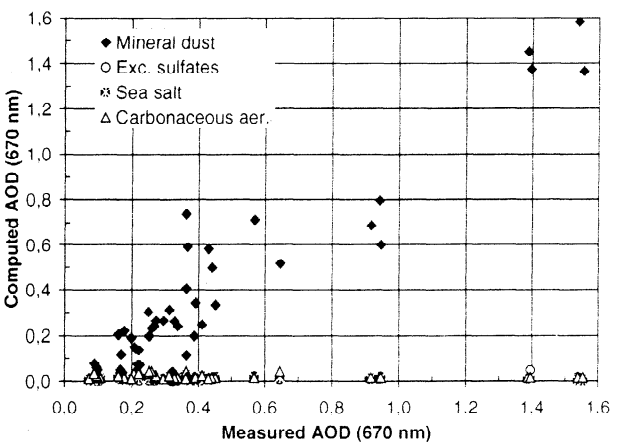

Figure 8. Aerosol optical depth computed for each aerosol component as a function of the measured aerosol optical depth at 670 nm.

5. Conclusions

The purpose of this study was to attempt a calculation of the AOD from the mass concentrations of the different aerosol species measured at ground level at Sal Island in order to evaluate their respective contributions to the total AOD over the northeastern tropical Atlantic. In this region we consider four major aerosol species, i.e., mineral dust of African origin, carbonaceous aerosols (including black carbon and particulate organic matter), sea salt particles, and excess sulfates. The concentrations of these aerosol species were continuously measured at ground level, and their vertical repartitions were derived from meteorological soundings. Because of the lack of continuous measurements, we account carbonaceous aerosol concentrations from average values on the basis of previous measurements performed at Sal Island from December 1991 to March 1992. To assess their respective optical effects, the specific extinction cross sections have been computed from the size distributions of each of these species derived from cascade impactor measurements, except for carbonaceous aerosols whose specific extinction cross sections have been assessed from the values provided by *Liousse et al.* [1996]. Because of the low relative humidity (<60 %) observed in this region, we assumed dry particles to retrieve aerosol optical properties. A satisfying agreement is obtained between the computed and the measured AOD at 670 nm during the experiment performed from mid-December 1994 to mid-February 1995 at Sal Island (less than 2% of error). However, besides this excellent agreement, it should be noted that this approach suffers from the lack of accurate measurements of vertical profiles of acrosol concentrations, which certainly remains a major source of uncertainty.

Nevertheless, the main interest of this approach is that it allows to quantify the contribution of each aerosol specie to the total AOD at 670 nm in the northeastern tropical Atlantic. Our results clearly show that mineral dust of African origin dominates both the aerosol mass load (average contribution of 71%) and the AOD (average contribution of 75% at 670 nm) in this region. Although sea salt particles contribute significantly to the aerosol mass load (24%), their effect on the AOD remains limited (6% on average, never exceeding 20 %) with a maximum optical depth of 0.02. This study also suggests that the effect of carbonaceous aerosols on the AOD could be significantly larger than the one of excess sulfates. Nevertheless, the average optical depth due to the sum of carbonaceous aerosols, excess sulfates, and sea salt

Table 3. Mean, Mimimum, and Maximum values of Measured and Computed AOD at 670 nm and Computed AOD for Different Aerosol Species

AOD, 670 nm	Measured	Computed				
	Total	Total*	Mineral Dust	Carbonaceous Aer.	Sea Salt	Excess Sulfates
Mean	0.42	0.41	0.36	0.02	0.012	0.008
Minimum	0.07	0.04	0.01	0.01	0.001	0.0002
Maximum	1.55	1.62	1.58	0.04	0.02	0.04

*Including a contribution of 0.007 for AOD due to stratospheric aerosol.

remains extremely limited (0.04 on average, never exceeding 0.1) in this region in comparison to the one due to mineral dust. The total AOD at 670 nm being rarely lower than 0.1, our results highlight that the optical effect of mineral dust is dominant in the northeastern tropical Atlantic not only during African dust events but also in most of the clear or moderate dustiness situations.

Acknowledgments. We wish to thank the site operators of the Servico Nacional de Meteorologia i Geofisica at Sal Island for collecting the aerosol samples. We also thank H. Cachier for collection of carbonaceous aerosol samples and L. Gomes especially for his help during field experiments. Thanks to C. Moulin for helpful comments. This work was supported by the "Programme National de Chimie de l'Atmosphère" (INSU/CNRS) and by the French Ministry of the Environment. This is LSCE contribution 161.

References

Andreae, M.O., Raising dust in the greenhouse, *Nature, 380,* 389-390, 1996.

Bergametti, G., R. Vie le Sage, B. Grubis, B. Dulieu, and C. Elichegaray, Relation between particle concentration in the atmosphere and aerosol collection efficiency, *Environ. Technol. Lett., 3,* 297-304, 1982.

Blanchard, D.C., and A.H. Woodcock, The production, concentration, and vertical distribution of the sea-salt aerosol, *Ann. N. Y. Acad. Sci., 80,* 330-347, 1980.

Bowen, H.J.M., Trace elements in biochemistry, *Academic, San Diego, Calif.*, 1966.

Brewer, P., Minor elements in seawater, in *Chemical Oceanography*, 2nd ed., vol. 1, edited by J.P. Riley and G. Skirrow, pp. 415-196, Academic, edited by San Diego, Calif., 1975.

Cachier, H., Combustion Carbonaceous Particles, R.M. Harrison and R. Van Grieken, John Wiley, in press, 1998.

Cachier, H., M.P. Brémond, and P. Buat-Ménard, Determination of atmospheric soot carbon with a simple thermal method, *Tellus*, Ser. B 41, 379-390, 1989.

Caquineau, S., Localisation des sources de poussières Sahariennes à l'aide de traceurs minéralogiques, *Ph.D. thesis, Univ. Paris 12*, 1997.

Carlson, T. N., and S.T. Benjamin, Radiative heating rates for saharan dust, *J. Atmos. Sci., 37,* 193-213, 1980.

Carlson, T.N., and J.M. Prospero, The large-scale movement of saharan air outbreaks over the Northern Equatorial Atlantic, *J. Appl.Meteorol., 11*, 283-297, 1972.

Chazette, P., C. David, J. Lefrere, S. Godin, J. Pelon, and G. Mégie, Comparative lidar study of the optical, geometrical, and dynamical properties of stratospheric post-volcanic aerosols, following the eruptions of El Chichon and Mount Pinatubo, *J. Geophys. Res., 100,* 23,195-23,207, 1995.

Chiapello, I., Les aérosols atmosphériques au-dessus de l'Atlantique nord tropical: Approche physico-chimique et météorologique. Evaluation de la contribution des différentes espèces à l'épaisseur optique en aérosol, *250 pp., Ph.D. thesis, Univ. Paris 7*, 1996.

Chiapello, I., G. Bergametti, L. Gomes, B. Chatenet, F. Dulac, J. Pimenta, and E. Santos Soares, An additional low layer transport of Sahelian and Saharan dust over the northeastern Tropical Atlantic, *Geophys. Res Lett., 22,* 3191-3194, 1995.

Chiapello, I., G. Bergametti, B. Chatenet, P. Bousquet, F. Dulac, and E. Santos Soares, Origins of African dust transported over the northeastern tropical Atlantic, *J. Geophys. Res., 102,* 13,701-13,709, 1997a.

Chiapello, I., G. Bergametti, J.P. Quisefit; and P. de Chateaubourg, Control and correction of the sample absorption effect in the analysis of atmospheric aerosol by X-ray fluorescence spectrometry, *Analusis, 25,* 141-147, 1997b.

Clarke, A.D., N.C. Ahlquist, and D.S. Covert, The Pacific marine aerosol: Evidence for natural acid sulfates, *J. Geophys. Res., 92,* 4179-4190, 1987.

d'Almeida, G.A., P. Koepke, and E.P. Shettle, Atmospheric Aerosols: Global Climatology and Radiative Characteristics, 561 pp., A. Deepak, Hampton, Va., 1991.

Dentener, F.J., G.R. Carmichael, Y. Zhang, J. Lelieveld, and P.J. Crutzen, Role of mineral aerosol as a reactive surface in the global troposphere, *J. Geophys. Res., 101,* 22,869-22,889, 1996.

Dulac, F., D. Tanré, G. Bergametti, P. Buat-Ménard, M. Desbois, and D. Sutton, Assessment of the African airborne dust mass over the western Mediterranean Sea using Meteosat data, *J. Geophys. Res., 97,* 2489-2506, 1992.

Gomes, L., G. Bergametti, F. Dulac, and U. Ezat, Assessing the actual size distribution of atmospheric aerosols collected with a cascade impactor, *J. Aerosol Sci., 21,* 47-59, 1990.

Hegg, D.A., J. Livingston, P.V. Hobbs, T. Novakov, and P. Russel, Chemical apportionment of aerosol column optical depth off the mid-Atlantic coast of the United States, *J. Geophys. Res., 102,* 25,293-25,303, 1997.

Holben, B.N., et al., AERONET—A Federated Instrument Network and Data Archive for Aerosol Characterization, *Remote Sens. Environ., 66,* 1-16, 1998.

Howell, S.G., and B.J. Huebert, Determining marine aerosol scattering characteristics at ambient humidity from size-resolved chemical composition, *J. Geophys. Res., 103,* 1391-1404, 1998.

Husar, R.B., L.L. Stowe, and J.M. Prospero, Characterization of tropospheric aerosols over the oceans with the NOAA advanced very high resolution radiometer optical thickness operational product, *J. Geophys. Res., 102,* 16,889-16,909, 1997.

Intergovernmental Panel on Climate Change (IPCC), Radiative forcing of climate change 1994, report from the Scientific Assessment Working Group (WGI), UNEP/WMO, Geneva, 1994.

Jaenicke, R., Aerosol physics and chemistry, in *Landolt-Börnstein Numerical Data and Functional Relationships in Science and Technology,* vol. 4b, edited by G. Fischer, pp. 391-457, Springer-Verlag, New York, 1987.

Jaenicke, R., and L. Schütz, Comprehensive study of physical and chemical properties of the surface aerosols in the Cape Verde Islands region, J. *Geophys. Res., 83,* 3585-3599, 1978.

Jäger, H., O. Uchino, T. Nagai, T. Fujimoto, V. Freudenthaler, and F. Homburg, Ground-based remote sensing of the decay of the Pinatubo eruption cloud at three northern hemisphere sites, *Geophys. Res Lett., 22,* 607-610, 1995.

Jankowiak, I., and D. Tanré, Satellite climatology of saharan dust outbreaks, *J. Clim., 5,* 646-656, 1992.

Junge C.E., *Air Chemistry and Radioactivity*, 382 pp., Academic, San Diego, Calif., 1963.

Koutrakis, P., and B.P. Kelly, Equilibrium size of atmospheric aerosols sulfates as a function of particle acidity and ambient relative humidity, *J. Geophys. Res., 98,* 7141-7147, 1993.

Li, X., H. Maring, D. Savoie, K. Voss, and J.M. Prospero, Dominance of mineral dust in aerosol light-scattering in the North Atlantic trade winds, *Nature, 380,* 416-419, 1996.

Liousse, C., C. Devaux, F. Dulac, and H. Cachier, Aging of savanna biomass burning aerosols: Consequences on their optical properties, *J. Atmos. Chem., 22,* 1-17, 1995.

Liousse, C., J.E. Penner, C. Chuang, J.J. Walton, H. Eddleman, and H. Cachier, A global three-dimensional model study of carbonaceous aerosols, *J. Geophys. Res., 101,* 19,411-19,432, 1996.

Liousse, C., F. Dulac, H. Cachier, and D. Tanré, Remote sensing of carbonaceous aerosol production by African savanna biomass burning, *J. Geophys. Res., 102,* 5895-5911, 1997.

Losno, R., G. Bergametti, and G. Mouvier, Determination of optima conditions for atmospheric aerosol analyses by X-ray fluorescence, *Environ. Technol. Lett., 8,* 77-87, 1987.

Moulin, C., F. Guillard, F. Dulac, and C.E. Lambert, Long-term daily monitoring of Saharan dust load over ocean using Meteosat ISCCP-B2 data, 1, Methodology and preliminary results for 1983-1994 in the Mediterranean, *J. Geophys. Res., 102,* 16,947-16,958, 1997a.

Moulin, C., C.E. Lambert, F. Dulac, and U. Dayan, Control of atmospheric export of dust from North Africa by the North Atlantic Oscillation, *Nature, 387,* 691-694, 1997b.

Moulin, C., F. Dulac, C.E. Lambert, P. Chazette, I. Jankowiak, B. Chatenet, and F. Lavenu, Long-term daily monitoring of Saharan dust load over ocean using Meteosat ISCCP-B2 data, 2, Accuracy of the method and validation using Sun photometer measurements, *J. Geophys. Res., 102,* 16,959-16,969, 1997c.

Nakajima, T., T. Tadahiro, A. Higurashi, G. Hashida, N. Moharram-Nejad, Y. Najafi, and H. Valavi, Aerosol optical properties in the Iranian region obtained by ground-based solar radiation measurements in the summer of 1991, *J. Appl. Meteorol., 35,* 1265-1278, 1996.

Patterson, E. M., D.A. Gillette, and B.H. Stockton, Complex index of refraction between 300 and 700 nm for Saharan aerosols, *J. Geophys. Res., 82,* 3153-3160, 1977.

Penner, J.E., R.J. Charlson, J.M. Hales, N.S. Laulainen, R. Leifer, T. Novakov, J. Ogren, L.F. Radke, S.E. Schwartz, and L. Travis, Quantifying and minimizing uncertainty of climate forcing by anthropogenic aerosols, *Bull. Am. Meteorol. Soc., 75,* 375-400, 1994.

Prospero, J.M., and T.N. Carlson, Vertical and areal distribution of Saharan dust over the western equatorial North Atlantic Ocean, *J. Geophys. Res., 77,* 5255-5265, 1972.

Prospero, J.M., D.L. Savoie, T.N. Carlson, and R.T. Nees, Monitoring saharan aerosol transport by means of atmospheric turbidity measurements, in *Saharan Dust Mobilization, Transport, Deposition SCOPE, Rep. 14,* pp. 171-186, edited by John Wiley, San Diego, Calif., 1979.

Quinn, P.K., S.F. Marshall, T.S. Bates, D.S. Covert, and V.N. Kapustin, Comparison of measured and calculated aerosol properties relevant to the direct radiative forcing of tropospheric sulfate aerosol on climate, *J. Geophys. Res, 100,* 8977-8991, 1995.

Quinn, P.K., V.N. Kapustin, T.S. Bates, and D.S. Covert, Chemical and optical properties of marine boundary layer aerosol particles of the mid-Pacific in relation to sources and meteorological transport, *J. Geophys. Res., 101,* 6931-6951, 1996.

Rahn, K.A., Silicon and aluminum in atmospheric aerosols: Crust-air fractionation?, *Atmos. Environ., 10,* 597-601, 1976.

Reid, J.S., P.V. Hobbs, C. Liousse, J.V. Martins, R.E. Weiss, and T.F. Eck, Comparisons of techniques for measuring shortwave absorption and black carbon content of aerosols from biomass burning in Brazil, *J. Geophys. Res.* in press, 1998.

Schwartz, S.E., and M.O. Andreae, Uncertainty in climate change caused by aerosols, *Science, 272,* 1121-1122, 1996.

Shettle, E.P., Optical and radiative properties of a desert aerosol model, in *Proceedings of a Symposium on Radiation in the Atmosphere,* edited by G. Fiocco, pp. 74-77, A. Deepak, Hampton, Va., 1984.

Sokolik, I.N., and O.B. Toon, Direct radiative forcing by anthropogenic airborne mineral aerosols, *Nature, 381,* 681-683, 1996.

Tanré, D., C. Devaux, M. Herman, R. Santer, and J.Y. Gac, Radiative properties of desert aerosols by optical ground-based measurements at solar wavelengths, *J. Geophys. Res., 93,* 14,223-14,231, 1988.

Tegen, I., and I. Fung, Contribution to the atmospheric mineral aerosol load from land surface modification, *J. Geophys. Res, 100,* 18,707-18,726, 1995.

Tegen, I., A.A. Lacis, and I. Fung, The inflluence on climate forcing of mineral aerosols from disturbed soils, *Nature, 380,* 419-422, 1996.

Vinogradov, A.P., *The Geochemistry of Rare and Dispersed Chemical Elements in Soils,* 2nd ed., Consult. Bur., Inc., New York, 1959.

World Climate Programme (WCP), Aerosols and Their Climatic Effects, edited by A. Deepak and H.E. Gerber, 107 pp., *Ser. Rep. 55,* Int. Counc. of Sci. Unions and World Meteorol. Organ., Geneva, 1983.

G. Bergametti and B. Chatenet, Laboratoire Interuniversitaire des Systèmes Atmosphériques, Universités Paris 7-Paris 12, UMR CNRS 7583, Créteil, France. (e-mail: bergametti@lisa.univ-paris12.fr; chatenet@lisa.univ-paris12.fr)

I. Chiapello and I. Jankowiak, Laboratoire d'Optique Atmosphérique, Université des Sciences et Technologies de Lille, Bat. P5, URA CNRS 713, 59655 Villeneuve d'Ascq Cedex, France. (e-mail: chiapello@loa.univ-lille1.fr; Isabelle.Jankowiak@univ-lille1.fr)

F. Dulac and C. Liousse, Laboratoire des Sciences du Climat et de l'Environnement, UMR CEA-CNRS, Gif sur Yvette, France (e-mail: dulac@lsce.saclay.cea.fr; catherine.liousse@lsce.cnrs-gif.fr).

E.S. Soares, Servico Nacional de Meteorologia i Geofisica, Sal, Cape Verde.

(Received April 22, 1998; revised September 23, 1998;
accepted October 1, 1998.)